Available online at www.sciencedirect.com
ScienceDirect
Remote Sensing of Environment 112 (2008) 75–93
Remote Sensing of Environment
www.elsevier.com/locate/rse

Spatially and temporally continuous LAI data sets based on an integrated filtering method: Examples from North America

Hongliang Fang [a,*], Shunlin Liang [a], John R. Townshend [a], Robert E. Dickinson [b]

[a] Department of Geography, University of Maryland, College Park, MD 20742, USA
[b] School of Earth and Atmospheric Sciences, Georgia Institute of Technology, Atlanta, Georgia, 30332, USA

Received 27 April 2006; received in revised form 19 July 2006; accepted 24 July 2006

Abstract

Leaf Area Index (LAI) is an important biophysical variable for characterizing the land surface vegetation. Global LAI product has been routinely produced from the MODerate resolution Imaging Spectroradiometer (MODIS) aboard the Terra and Aqua satellite platforms. However, the MODIS standard LAI product is not continuous both spatially and temporally. To fill the gaps and improve the quality, we have developed a data filtering algorithm. This filter, called the temporal spatial filter (TSF), integrates both spatial and temporal characteristics for different plant functional types. The spatial gaps are first filled with the multi-year averages of the same day. If the values are missing over all years, the pixel is filled with a new estimate using the vegetation continuous field–ecosystem curve fitting method. The TSF integrates both the multi-seasonal average trend (background) and the seasonal observation. We implement this algorithm using the MODIS Collection 4 LAI product over North America. Comparison of the TSF results with the Savitzky–Golay filter indicates that the TSF performs much better in restoring the spatial and temporal distribution of seasonal LAI trends. The new LAI product has been validated by comparing with field measurements and the derived LAI maps from ETM+ data at a broadleaf forest site and an agricultural site. The validation results indicate that the new LAI product agrees better with both the field measurements and LAI values obtained from the ETM+ than does the MODIS LAI standard product, which usually shows higher LAI values.

Keywords: Leaf area index (LAI); Moderate Resolution Imaging Spectroradiometer (MODIS); Temporal and spatial filter; Remote sensing; Terra; Ecosystem curve fitting (ECF)

1. Introduction

Leaf area index (LAI) is being provided by the science team from observations acquired by the MODerate resolution Imaging Spectroradiometer (MODIS) instruments aboard NASA's Terra and Aqua satellites. However, the current LAI product is spatially and temporally discontinuous due to cloud cover, seasonal snow and instrument problems. This limits the application of LAI in ground surface process simulation, climatic modeling and global change research. Modelers would want continuous high quality data that can be used easily. While the QC (quality control) layers have some value, they need to be explored further in order to provide the highest quality data.

To enable these LAI products to be used with their various kinds of gaps, it is intuitively appealing to use either temporal or spatial filters. Several mathematical filters have been used to fill gaps in remotely sensed data, such as simple linear interpolation, best index slope extraction (Viovy et al., 1992), Fourier wave adjustment (Sellers et al., 1994), polynomial fitting (Karnieli et al., 2002), Asymmetric Gaussian filter (Jönsson & Eklundh, 2002), Savitzky–Golay filter (Chen et al., 2004; Savitzky & Golay, 1964), or piecewise logistic function fitting (Zhang et al., 2003). These methods have been mainly used to restore the NDVI (normalized difference vegetation index) profile (Cihlar, 1996; Sellers et al., 1994), but they can also be used for LAI with some adjustments.

Spatial filtering using pixel-level or regional ecosystem statistical data is provided by most commercial image processing software. Various spatial filters have long been adopted in digital data processing to remove noise or enhance surface features. Geostatistical methods, such as co-kriging and stochastic

* Corresponding author. Now at NASA Goddard Earth Sciences Data and Information Services Center (GES DISC) employed by RS Information Systems, Inc., McLean, Virginia, USA. Tel.: +1 301 614 5512; fax: +1 301 614 5268.
E-mail address: hfang@geog.umd.edu (H. Fang).

0034-4257/$ - see front matter © 2007 Elsevier Inc. All rights reserved.
doi:10.1016/j.rse.2006.07.026

Table 1
The MODIS LAI quality control (QC) values and algorithms and the TSF algorithm treatments

QC values	SCF_QC (binary, decimal values)	MODIS LAI algorithms	TSF algorithms	
			Background	Observation
QC<32	000=0	Main (RT) method with the best possible results	Good data (not processed)	
32<=QC<64	001=1	Main (RT) method with saturation	Multi-year average or	Use original MODIS LAI
64<=QC<96	010=2	Empirical method used (Main method failed due to geometry problems)	VCF–ECF method	as observation
96<=QC<128	011=3	Empirical method used (Main method failed due to problems other than geometry)		
QC>=128	100=4	Couldn't retrieve pixel		Temporal filtering

SCF_QC are the binary bits indicating LAI algorithms.

Table 2
Filled values in the standard MODIS LAI Collection 4 product

Filled values	Description
255	Not-computed or outside projection
254	Water (Ocean or inland)
253	Barren, very sparsely vegetated
252	Perennial snow or ice on pixel
251	Permanent wetlands, marshes
250	Urban, built-up areas
249	Unclassified

simulation, have been used for mapping vegetation variables (Dungan, 1998). Berterretche et al. (2005) reviewed several aspatial and spatial methods and compared reduced major axis, kriging with an external drift and sequential Gaussian conditional simulation to develop continuous LAI maps over a boreal forest study site. Nevertheless, techniques based purely on spatial methods are very limited because there are usually large regions that have poor spatial coverage, which cannot readily be filled. Furthermore, simple spatial filtering of an ecosystem may fail to represent the complexity of real landscapes. Ecosystem statistics only indicate the general characteristics of a small region, they cannot represent the spatial structure and continuous gradations that characterize real landscapes.

Moody et al. (2005) tried to combine both temporal and spatial methods and developed an ecosystem-dependent temporal interpolation technique to fill missing or snow-covered pixels in the MODIS albedo data product. The shapes of the pixel's and region's ecosystem phenological curves are determined first (Moody et al., 2005). The method imposes pixel and regional ecosystem phenological profile onto the target pixel's temporal data to maintain pixel-level spatial and spectral detail and integrity (Moody et al., 2005). This ecosystem curve fitting (ECF) method uses both spatial and temporal information to derive value-added data sets.

The ECF method cannot be simply applied to LAI products for several reasons. First, LAI is an 8-day composite product and its temporal curve is not as smooth as other daily products. There are realistic variations that look like outliers, for example those associated with crops in the growing season. Second, the LAI profile from the pixels with the same ecosystem classification may not represent the pixel itself. This is mainly due to the coarse land surface classification that is still problematic for mixed pixels. For example, 'cropland' could include corn, soybean or the mixture of the two. The ECF method assumes there are no mixed pixels for all the ecosystem classes. Most importantly, for the same ecosystem, their LAI could vary widely within a short distance due to different vegetation densities. For example, the tree cover of central Maryland, USA (15–45%) is about half of the typical temperate forest (50–90%) in the surrounding mountains (DeFries et al., 2000). Their albedos are very similar, but their LAI could differ by 2.0–3.0 (Fang & Liang, 2005). One of our studies in a semi-arid area also illustrates the problem of using the regional ecosystem average (Fang et al., 2005). The land cover maps label the study area as 'shrub'; however, the area is composed of about 20–30% trees, 20–30% grasses and 50% bare ground (Fang et al., 2005). Obviously, errors will be introduced to the ECF method if the vegetation fraction is not accounted in the curve fitting procedure.

The objective of this paper is to develop a filtering algorithm that aims to fill spatial and temporal gaps and improve bad quality values from contextual data (in space and time). In addition to many missing values, a significant amount of the MODIS LAI data is retrieved from the backup algorithm. We will first analyze

Table 3
Percentage of MODIS LAI product with different Quality Control flags for North America during 2000–2004

	PFTS	1	2	3	4	5	6	7	8	9	10	11
SCF_QC	0	47.6	37.8	43.2	43	59	57.8	54.3	53.8	48.7	22.3	41.1
	1	2	7.1	1.6	5.5	0.4	1	2.5	2.2	0.5	2.6	0.6
	2	5.1	4.7	5.3	4.6	5.4	5.1	5.7	4.1	3.4	1.4	4.3
	3	19.5	27.3	16.5	23.9	14.1	15.8	18	16.9	8.7	23.4	13.3
	4	25.8	23.1	33.3	22.9	21.1	20.2	19.5	23	38.7	50.3	40.7
Retrieval index		71.8	62.2	73.1	67	80.8	78.8	75.9	76.8	85	51.6	75.8

PFTs shows different plant functional types with 1–11 correspond to (a)–(k) in Fig. 1.
RI (Retrieval index)=(SCF_QC0+SCF_QC1)/(SCF_QC0+SCF_QC1+SCF_QC3).

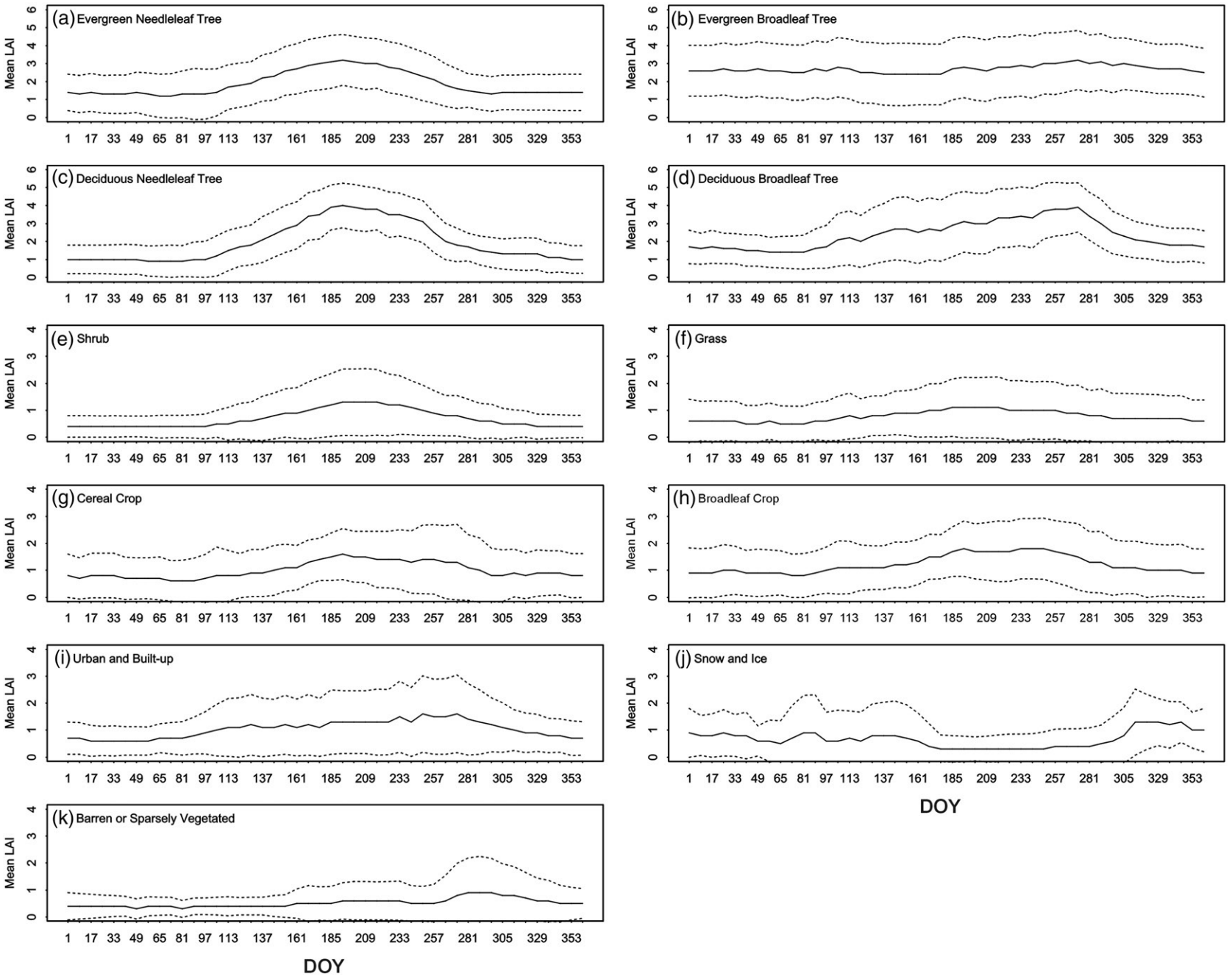

Fig. 1. Seasonal variation of North America MODIS LAI from 2000 to 2004. The multiple year LAI average (solid line) was obtained from five years' 8-day best quality (QC < 32) LAI directly (not from the average of means). The dashed lines are the mean LAI ± one standard deviation. DOY: Day of the year.

the MODIS LAI product in this section. The new spatio-temporal filter will be described in Section 2, followed by the filtered results and their validation in Sections 3 and 4, respectively.

1.1. The MODIS LAI product

Surface ecosystems are represented as patches of plant functional types (PFTs). The MODIS land cover classification products provide the plant functional type (land cover type 5) in consideration of the Community Land Model used in climate modeling. The MODIS 1 km PFT map consists of 11 primary PFTs: evergreen needleleaf and broadleaf trees, deciduous needleleaf and broadleaf trees, shrub, grass, cereal and broadleaf crops, urban and built-up, snow and ice, barren or sparsely vegetated. PFTs provide a direct linkage to leaf-level ecophysiological measurements and ecological theory (Bonan et al., 2002). Models of vegetation dynamics and biogeography routinely use PFTs to represent the surface landscapes (Haxeltine & Prentice, 1996; Running & Gower, 1991; Running & Hunt, 1991). Here we assume that each 1 km pixel has only one PFT. The MODIS land cover product does provide a secondary class and the percent of the secondary class, but this class was not considered since there is no confidence level or QC data associated with it.

To examine the global MODIS LAI product, quality control flags need to be consulted (Table 1). Non-vegetated areas are filled with different values (Table 2). Globally, about 67% of pixels are retrieved by the main radiative transfer algorithm and the others by the backup algorithms for the current collection 4 product (Yang et al., 2006). We have also examined the five-year (2000–2004) MODIS collection 4 1-km LAI product and its QC layers for North America. In North America, less than half of the land areas (48.6%) are retrieved successfully by the main radiative transfer method during the 2000–2004 period, lower than the global average. For shrub, only 59.4% is retrieved by the main radiative transfer method during the period, the highest among all the plant functional types (PFT5 in Table 3). The retrieval index, the ratio of the number of pixels retrieved by the main algorithm to the total number of retrievals by both the main and backup algorithms, is often used to represent the data retrieval quality (Wang et al., 2001). The retrieval indices for the herbaceous types (0.808, 0.788, 0.759, 0.768 for shrub, grass, cereal and broadleaf crops, respectively) were all higher than those of the trees (0.718, 0.622, 0.731 and 0.67 for the evergreen needleleaf, evergreen broadleaf, deciduous needleleaf, and deciduous broadleaf trees, respectively). The highest and lowest retrieval indices were observed for urban/built-up and snow/ice types, respectively (0.85 and 0.516). For barren or sparsely vegetated area, the retrieval index was also higher (0.758) than for trees.

For pixels retrieved with the main RT method with the best possible results (QC < 32), their values are used as references and kept in the output. Fig. 1 shows the seasonal variation of MODIS LAI from 2000 to 2004 for different PFTs. The average values (solid lines) were obtained from five years' 8-day best quality (QC < 32) LAI directly. Our algorithm mainly targets low quality and missed pixels. To calculate the background value, the pixel's multi-year average was used to fill the missing pixels. If the multi-year average does not exist, an improved VCF–ECF method will be applied. If no values exist in the MODIS LAI product, a temporal filter is activated to calculate the observational values. The new filter combines both background and observational information in order to generate improved products.

2. Description of the temporal and spatial filter (TSF)

2.1. Theoretical basis

Considering the case of a single observation at location r_j, two estimates are used for the analysis: 1) the background value at the gridpoint r_i and 2) the difference between the observation $x_o(r_j)$ and the background $x_b(r_j)$ plus $x_o(r_i)$. It is recognized that both the background and the observation estimates contain errors. In this case, instead of using a simple geometric function to calculate the weight, the uncertainties of the background and observation are included in the weighting function. These two estimates can be weighted in an optimal way (Bergthorsson & Doos, 1955) to calculate the target value $x_a(r_i)$:

$$x_a(r_i) = \frac{E_b^{-2}x_b(r_i) + E_o^{-2}w(r_i, r_j)\{x_b(r_i) + [x_o(r_j) - x_b(r_j)]\}}{E_b^{-2} + E_o^{-2}} \quad (1)$$

Where E_b^2 and E_o^2 are the error variance for the background and observation, respectively. Both the background error and

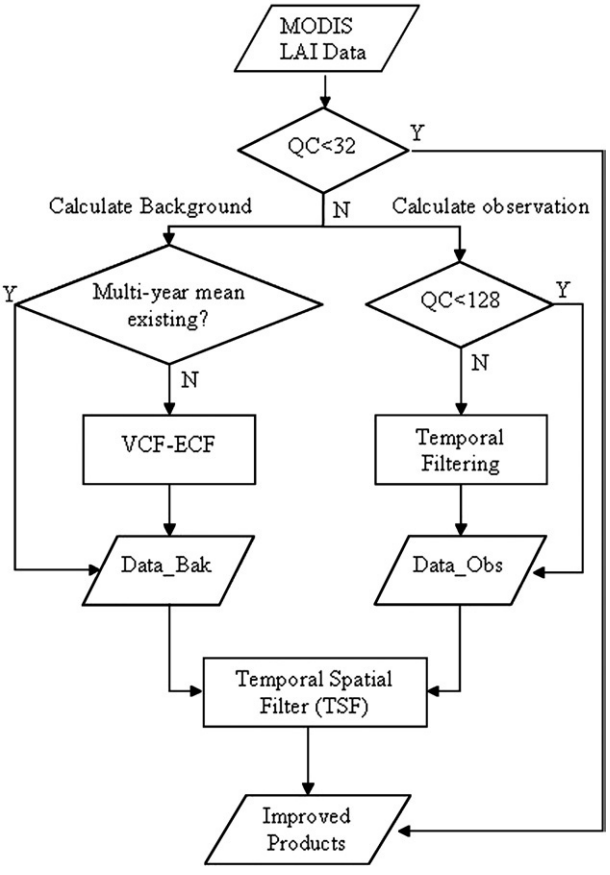

Fig. 2. Flowchart of the temporal spatial filtering (TSF) process. QC stands for the MODIS quality control flag.

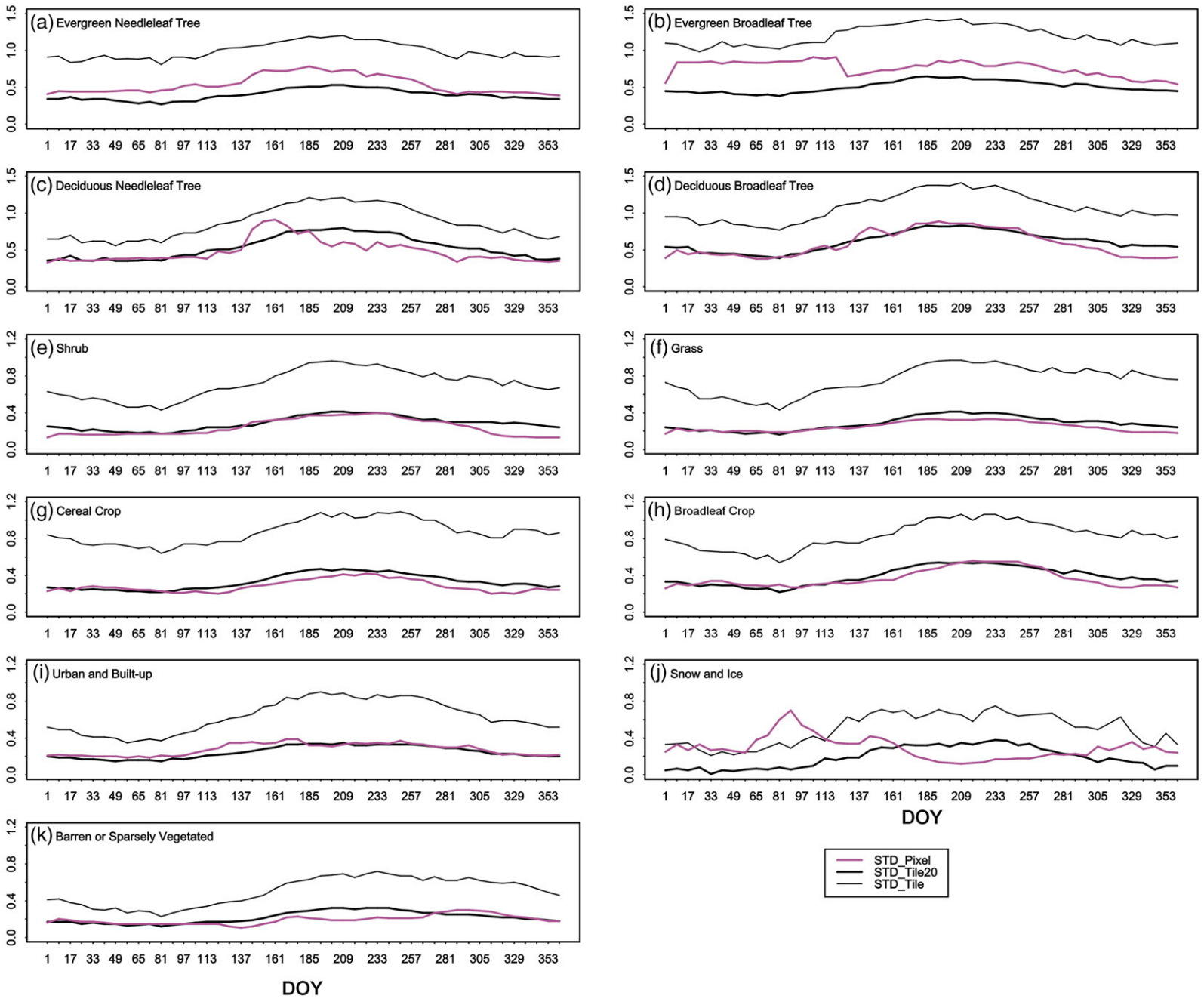

Fig. 3. Comparison of standard deviation (STD) for different pixels (pink lines) and PFTs (dark lines). "_Pixel" are multi-year statistics for each pixel and are clustered into different PFTs for display. The statistics of different PFT were calculated at tile level. "_Tile" represents all pixels in the tile, and "_Tile20" only pixels within ±20% of VCF range in the tile. Only best quality LAI data (QC < 32) were considered.

observation error are assumed homogeneous and spatially uncorrelated and E_b^2 and E_o^2 are assumed independent of location. $w(r_i,r_j)$ is the weighting function dependent on the time distance $d_{i,j}$ between points r_i and r_j

$$w(r_i, r_j) = \max\left(0, \frac{R^2 - d_{i,j}^2}{R^2 + d_{i,j}^2}\right) \quad (2)$$

where R is a predefined radius of influence. An $R=16$, i.e., two MODIS LAI data cycles in the neighborhood, is used in this paper. If the two estimates are at a specific location on the same day (i.e., $r_i=r_j$, and $w(r_i,r_j)=1$), Eq. (1) takes a simplified form as:

$$x_a(r_i) = \frac{E_b^{-2} x_b(r_i) + E_o^{-2} x_o(r_i)}{E_b^{-2} + E_o^{-2}} \quad (3)$$

Based on the above rationale, a three-step filtering technique is developed to produce spatially and temporally continuous products from existing discontinuous ones. Fig. 2 shows the general process of the temporal spatial filter (TSF):

1) Temporal filling. The missing pixel is filled with its multi-year average first. This initial step is based on the fact that the pixel's multi-year variation is less than or similar to the spatial variation within an ecosystem (Section 2.2);
2) Applying an improved ecosystem curve fitting (ECF) method based on the MODIS vegetation continuous fields product (VCF) (Hansen et al., 2003). In contrast to the existing ECF method, the new VCF–ECF method imposes regional VCF-dependant phenological behavior onto each target pixel's temporal data in order to maintain pixel-level spatial and temporal integrity (Section 2.2.1);
3) Calculation of the observation value. In general, the MODIS standard LAI data are used as the observation. However, if the data are missing (QC > 128), a temporal filter will be triggered to obtain the observed value (Section 2.3).
4) Combined temporal and spatial filtering. Using the results from the above steps as the background and observation values, an integration formula (Eq. (1)) is designed to integrate the pixel's multi-year trend and yearly variation and obtain the target value.

In the following sections, we will discuss how to calculate the background and observation values and their error variance.

2.2. Calculation of the multi-year variation (background)

Is the spatial average (within a PFT) or temporal average (over multiple years) the best "background" value? To answer this question and to demonstrate the feasibility and reliability of the

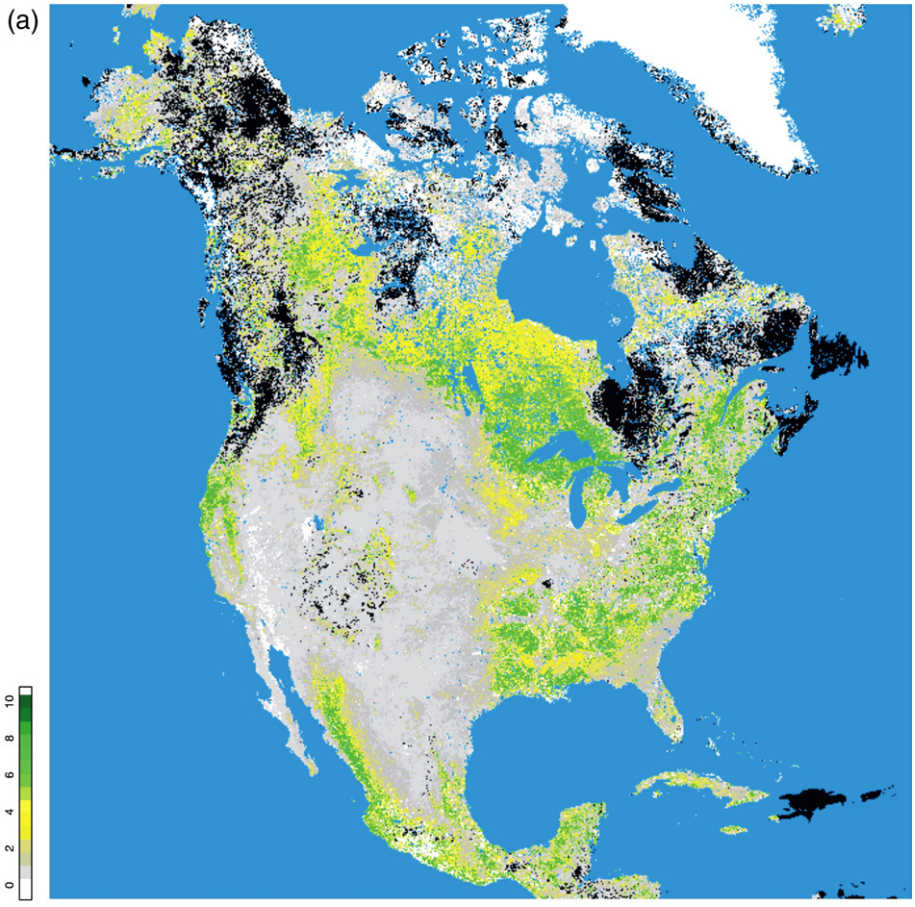

Fig. 4. Comparison of MODIS LAI maps before and after filtering (day 225, 2000). (a) MODIS standard LAI data; (b) after SG filtering; (c) New value-added MODIS LAI data sets after TSF.

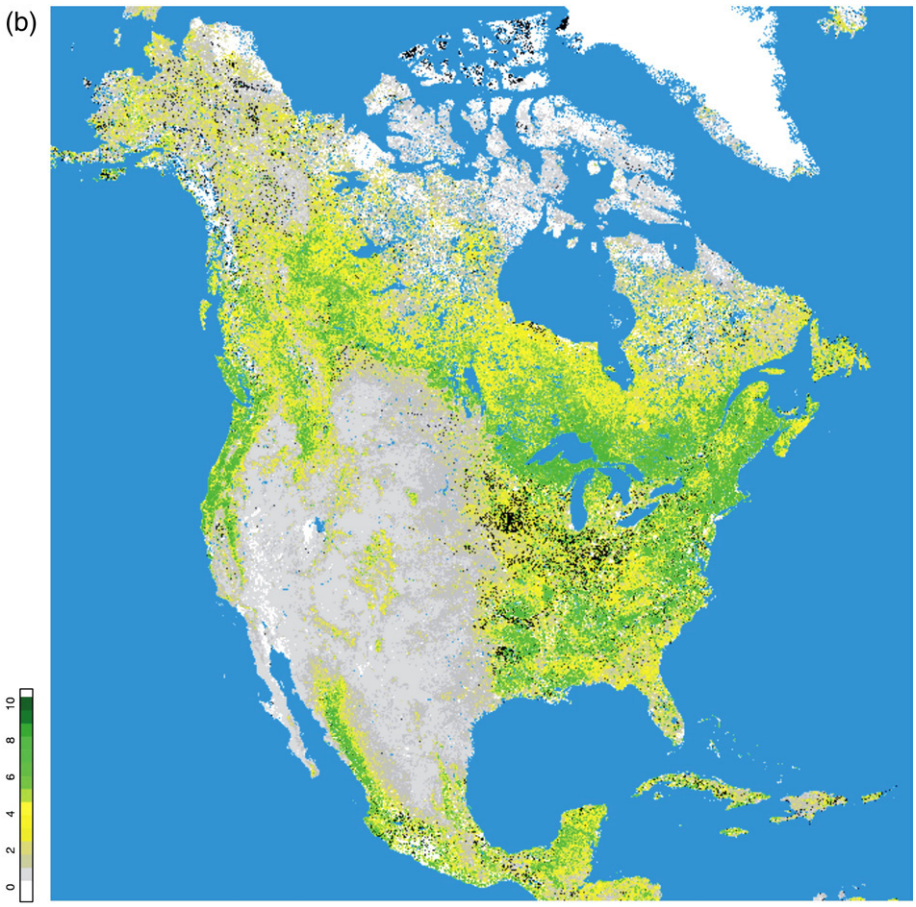

Fig. 4 (*continued*).

proposed method, it is necessary to compare the product's variation over different years (pixel level) and within an ecosystem. For ease of computation, we compared the standard deviation (STD) and coefficient of variation (CV) at both pixel and tile levels. The MODIS LAI products are reprojected on the Integerized Sinusoidal 10-degree grid, where the globe is tiled into 36 tiles along the east–west axis, and 18 tiles along the north–south axis. At the pixel-level, the STD and CV are first calculated over multiple years for a single pixel and then averaged for each plant functional type. At the tile level, the STD and CV are first calculated within a tile for each PFT and then averaged over the study area for multiple years.

Fig. 3 compares the STD at both temporal and spatial dimension for different PFTs. The pink line shows the STD of a pixel over multiple years (STD_Pixel). The thinner dark line shows the STD of different PFT within a tile (STD_Tile). The multi-year STD has a strong seasonal trend. For vegetation, it is lower in winter and spring, and increases during the growing season. For most PFTs, the yearly STD is consistently lower than the tile STD. The only exception is for snow and ice, which has a higher yearly STD in the spring because of different thaw dates. The CV shows the same phenomena (not shown here). This finding supports our assumption that a multi-year average is more representative and stable than the ecosystem average. Using the sinusoidal tile systems, the mean values of each PFT over the same latitude zone (10°) were calculated. Both STD and CV were examined at different latitude zones at pixel and tile levels (not shown here). The finding is the same as previously and is more remarkable at higher latitudes (>50°).

The LAI gaps were first filled with multi-year mean values. Five years of MODIS standard LAI data (2000–2004) were calculated. The mean value map illustrates the expected LAI value of a pixel at a certain time of year. The variance of LAI is interpreted as uncertainty for the LAI estimation. It was calculated for each PFT in a tile. The variances for patches of good and poor input pixels were calculated separately. In Fig. 2, the multi-year average is considered first. When pixel values are missing over all years and thus such multi-year average does not exist, the ECF method is applied as described next.

2.2.1. The ECF and VCF–ECF methods

The ecosystem curve fitting (ECF) is essentially a unique spatial filtering technique. To provide the pixel's missing data, the shape of the curves is imposed onto the pixel's valid temporal data by computing an average offset between pixel data and the behavioral curves. The ECF method is crucial, in cases where all five-year data are missing for some pixels and the variation within the ecosystem is relatively small (STD_Tile<STD_Pixel). The existing ECF method was improved based on the vegetation continuous field (VCF) data in case of high within-ecosystem

Fig. 4 (*continued*).

heterogeneity (STD_Tile > STD_Pixel). The VCF data were used to circumvent the difficulties of large LAI variations within an ecosystem. VCF provides continuous field representations of the heterogeneous gradations in land cover that characterize much of the Earth's surface. For many applications, such as physical models of land surface dynamics, a continuous field provides a more accurate representation of the land surface than does a simplified thematic land cover class with discrete boundaries (Small, 2004). The MODIS VCF product contains the percentage of trees, bare, and herbaceous which add up to represent 100% ground cover (Hansen et al., 2003).

We have illustrated that the multi-year STD and CV are constantly less than that of the ecosystem variation (Fig. 3). If VCF is considered, the ecosystem STD and CV could be greatly reduced. If a pixel's value is missing, it is filled with the ecosystem average calculated from pixels with similar VCF (e.g. within a certain VCF interval $\pm\alpha$). For computational efficiency, a PFT's average value for different VCF intervals (α=10%, 20%, 30%, …) within a tile are calculated first. The average LAI value calculated from a lower α is preferred for missing pixels. If it does not exist, a wider interval is searched, starting from 10%. Statistics show that the average PFT values are much more stable when VCF is imposed (Fig. 3, STD_Tile20). Statistics calculated from different α values were compared. The 20% VCF interval was found very feasible for this application and the STD and CV were close to the multi-year variations (Fig. 3, STD_Tile20).

The North America MODIS VCF data in 2001 (1 km) were used (http://glcf.umiacs.umd.edu/data/modis/vcf/).The MODIS VCF data are available in Goodes' projection or latitude/longitude. The VCF–ECF module is activated if there is no QC < 32 observation over all years and when the CV_Tile is higher than the CV_Pixel.

2.3. Calculation of the observational value

The above section calculates a 'background' value x_b in Eq. (1) for each pixel. To use Eq. (1) for calculating the new estimate, we also need an observed value (x_o). The original MODIS LAI data can be treated as the observed value. When 32 <= QC < 128 (using the back-up algorithm), they are treated as the observation. The variance of LAI is calculated with the same quality label within the particular PFT. Based on our rationale in Section 2.1, it's logical to obtain the observational variance for each pixel. In practice, the particular PFT's variance within the tile is used for simplicity. When QC > 128, there is no retrieval and a local temporal filter is necessary to obtain the 'observed' value from the neighboring best values (Table 1). If no best QC is available in the neighborhood, the background values will be used in the temporal filter. After evaluating several common temporal filters, we applied the Savitzky–Golay (SG) filter (Chen et al., 2004; Savitzky & Golay, 1964) and their coefficients (windows size N=5) in this study. The SG filter was selected here

because of its insensitivity to outliers and capability for full automation. It is also easy and fast to implement for a large area and has worked well for NDVI filtering (Chen et al., 2004). The combined variance is calculated with

$$E_o^2 = \frac{\sum_{k=1}^{N} C_k E_k^2}{\sum_{k=1}^{N} C_k} C_k \quad (4)$$

Where C_k is the coefficient of the SG filter and E_k^2 is the variance of the kth day in the temporal filter. A *posteriori* readjustment of the filtered SG curve is generally used in other application of the SG filter for the NDVI profile (Chen et al., 2004); however, it was not applied in this paper because the readjustment will lead to an LAI overestimation. Note the SG filter was applied locally, not the seasonal application done below for comparison (Section 3.3). In addition, the SG filter will malfunction when the temporal gaps are bigger than half the window size. In this case, a linear interpolation is suggested.

At higher latitudes (>50°), there are large areas marked 'no retrieval' in the MODIS LAI products in the spring due to persistent clouds and snow coverage. Even if there are some LAI retrievals, the data quality is ubiquitously low. To approximate the observation information, the ecosystem curve fitting algorithm was used (Moody et al., 2005). Moreover, a large amount of sparsely vegetated areas were found to have been assigned the filled values due to the failure of the MODIS retrieval algorithm. However, these are crucial ecosystems and have been fully processed using our algorithm.

3. Results

We present below the results of our filtering method on LAI values over North America, followed by their climatologies for different plant functional types. The TSF results were compared with those from the Savitzky–Golay (SG) filter (Chen et al., 2004; Savitzky & Golay, 1964) for all of North America. To reduce the effort of reprojecting the tiles with their sinusoidal (SIN) projection, the LAI were calculated tile by tile. The final results were reprojected to Lambert Azimuthal Equal-Area (LAEA) for North America from which they can be easily transformed to other projections.

For visualization purposes, a simplified projection look-up table was developed to facilitate the usually time-consuming reprojection process. Since a pixel's coordinates in the new projection system and its position in a tile are similar to a multiple-to-one match, a projection table was created with four columns. The first two columns are the coordinates in the new projection systems, and the other two columns represent the positions in a

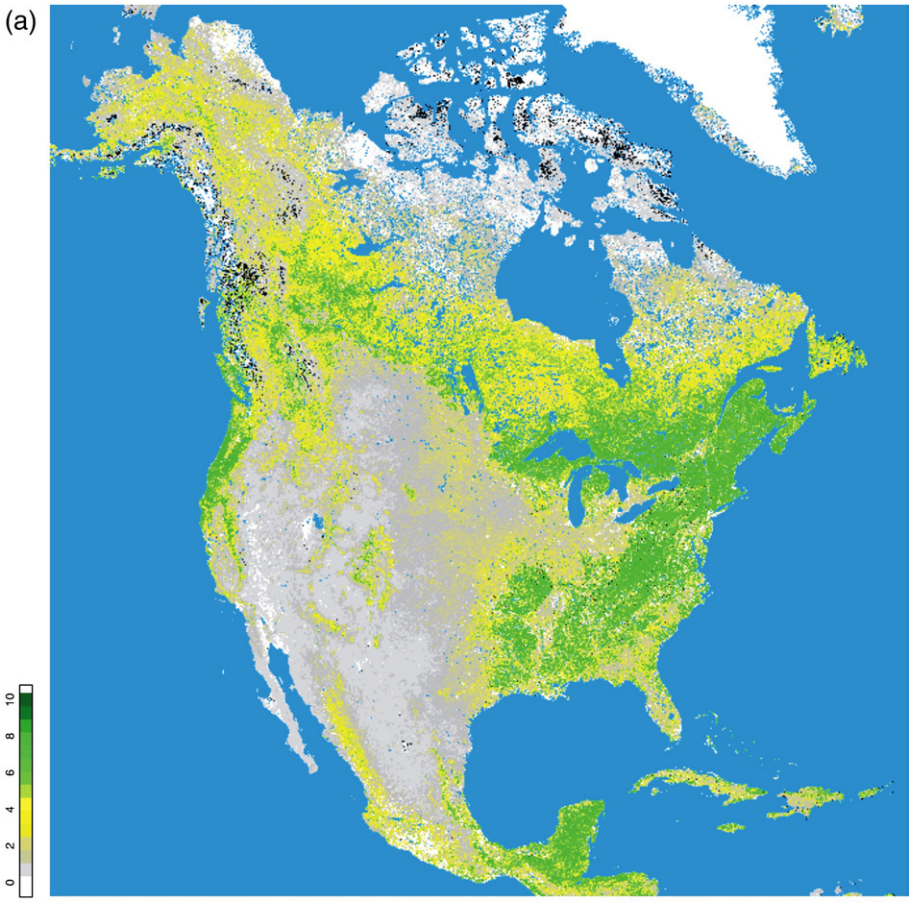

Fig. 5. New reconstructed LAI data sets with different methods (day 169, 2001): (a) the Savitzky–Golay filter; (b) the new TSF method.

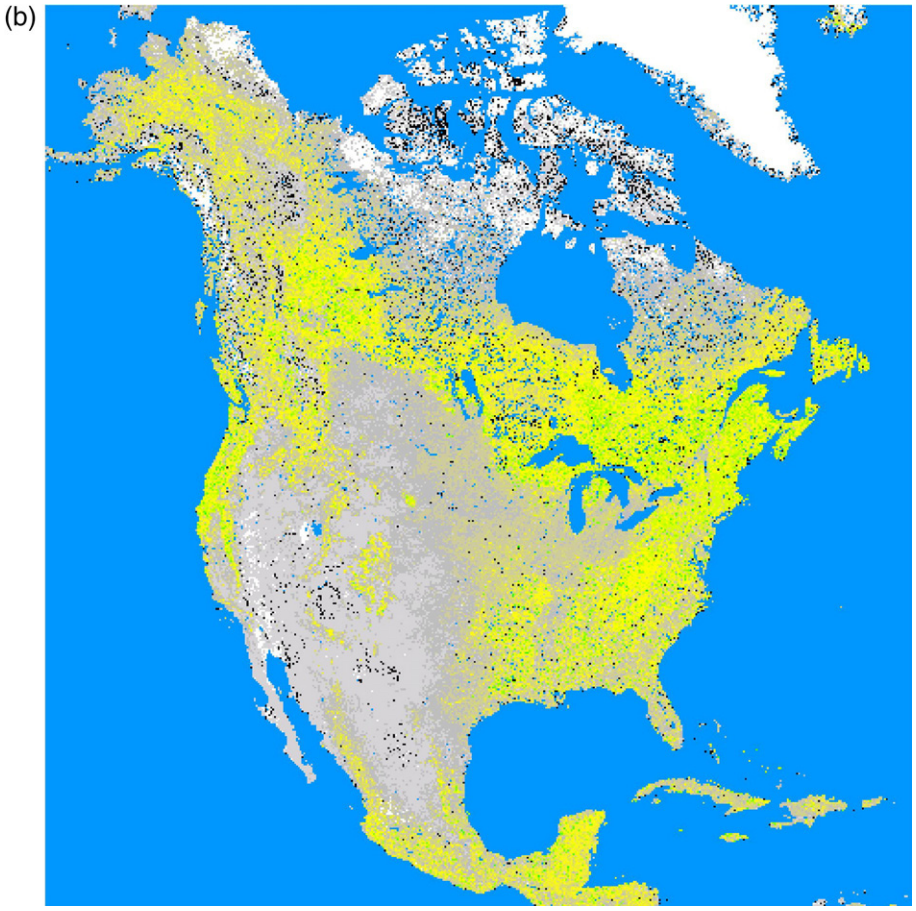

Fig. 5 (*continued*).

particular sinusoidal tile. Thus, the complicated reprojection and resampling process is simplified as a general file read and write process.

3.1. Spatially complete LAI products for North America

Fig. 4 shows the MODIS standard LAI data and the improved LAI products over North America on day 225, 2000. The white colored pixels are non-vegetated areas, such as perennial snow, ice and urban areas, corresponding to the filled values in Table 2. The MODIS standard LAI data were of very low quality due to large cloud coverage (black pixels in Fig. 4). This is even serious at high latitudes (>50°). We have greatly improved the data quality and their utility, especially at high latitudes (Fig. 4c) where the majority of pixels have no valid retrieval. Our new products are spatially complete. Visually, the TSF results generally produced considerably lower LAI values than the original product (Fig. 4). For example, around the Great Lakes Fig. 4a shows LAI about 6–8 whereas Fig. 4c shows LAI about 4–5. However, in the mid-west states (broadleaf crops), the TSF results increased the original LAI values by about 1.0–1.5. Improvements are also observed in the Appalachian mountains with more continuous values corresponding with landscapes.

The results for year 2001 are shown in Fig. 5. In year 2001, there is no LAI data on day 169 due to instrument problems. The LAI of this day was successfully restored with the TSF technique (Fig. 5b).

3.2. LAI climatologies for North America

The land product climatologies provide reasonable estimates for surface and atmospheric model variables. Fig. 6 displays the LAI climatologies before and after filtering in 2001. The mean value (solid thick lines) for each plant functional types is shown. For comparison, the MODIS standard LAI product is also displayed including those from the main radiative transfer (RT) algorithm (LAI_QC<32, thin solid lines) and those from both the RT and backup algorithms (LAI_QC<128, thin dashed lines) (Fig. 6).

In general, after the filtering, the new products have greatly improved the quality of the original data products by filling gaps and smoothing spikes. For vegetation, the LAI_TSF climatologies display clearly a seasonal growing trend. The standard deviation for each variable was also examined (not shown in the figure) and was found to be higher in the summer and lower in the winter.

For forests, the TSF results are in very good agreement with the original LAI_QC<32 for each PFT. The MODIS LAI retrieved from the main algorithm (LAI_QC<32) is usually lower than the overall mean value (LAI_QC<128), especially for

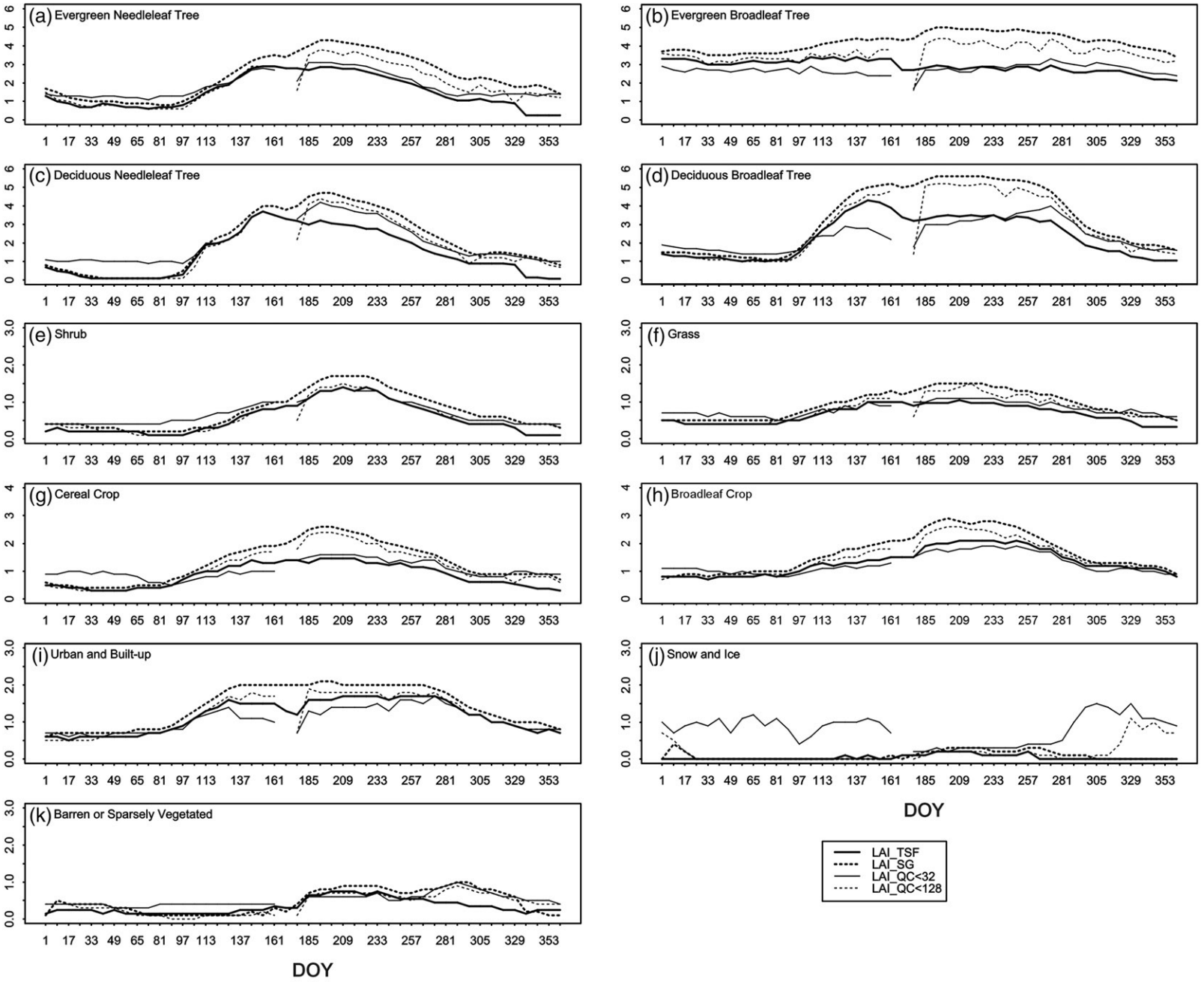

Fig. 6. LAI climatology for North America in 2001. Mean LAI values are calculated from the best (QC < 32) and the overall MODIS LAI products (QC < 128), respectively. The LAI time series after the SG filtering (thick dotted line) and the TSF method (thick solid line) are illustrated.

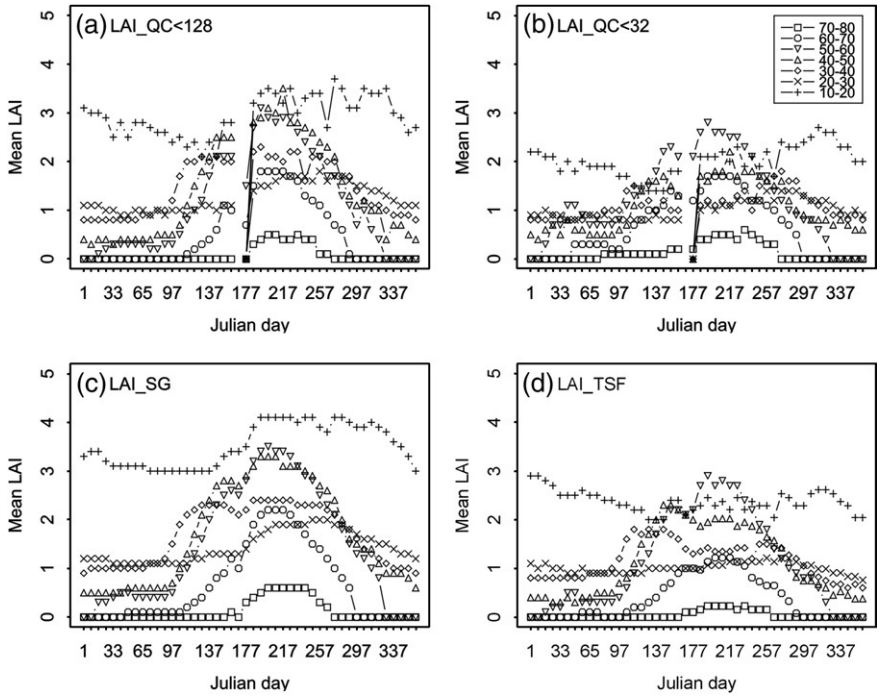

Fig. 7. LAI time series at different latitude bands in 2001. (a) LAI_QC<128; (b) LAI_QC<32; (c) SG; (d) TSF.

evergreen and deciduous broadleaf trees (Fig. 6b and d). For both evergreen and deciduous needleleaf trees, the LAI_TSF produced very similar results to the MODIS LAI products (Fig. 6a and c). The climatology is abnormally low in January, however, due to the very poor quality in the original data set. There are no valid MODIS LAI data at higher latitudes (>50°) for the spring of 2000–2003. For both evergreen and deciduous broadleaf trees, the LAI_TSF is lower than the overall average (LAI_QC<128), but very close to the LAI_QC<32 during some periods. For the evergreen broadleaf trees, the LAI_TSF line is smooth and usually larger than the LAI_QC<32 by about 1.0–1.5 for most of the year (Fig. 6b). The biggest difference lies in the deciduous broadleaf trees (Fig. 6d). In the original products, the LAI_QC<128 is much higher than the LAI_QC<32. For deciduous broadleaf trees, the early summer green-up is much clearer in the TSF products, while it was much elongated in the LAI_QC<32 (Fig. 6d). Differences between the LAI_QC<32 and LAI_QC<128 also reveal the potential uncertainties in the MODIS LAI data products.

For herbaceous vegetation, the TSF results are very close to the standard LAI values, especially for grass, shrub, barren or sparsely vegetated areas (Fig. 6e,f,k). This is partly due to the high quality of the original MODIS LAI products. Other research has shown that the MODIS LAI is more robust for herbaceous vegetation types (Cohen et al., 2003; Fang & Liang, 2005; Yang et al., 2006). However, there are some noticeable deviations for cereal and broadleaf crops in the summer, when the LAI_QC<32 is lower than the overall average by about 1.0. During this period, the TSF climatology is between that of the best and overall MODIS LAI products (Fig. 6g and h).

For the urban and built-up area, our product is closer to the overall climatology (Fig. 6i). The differences between the LAI_QC<32 and LAI_QC<128 illustrate the complexity of this cover types and uncertainties of the standard LAI. For snow and

Table 4
Field sites used for LAI intercomparison of the MODIS LAI and our filtered LAI

#	Name	Biome class	Latitude	Longitude	Method	Database or reference
1	Bondville	Broadleaf crop	40.007	−88.291	Destructive harvest	BigFoot
2	Konza	Grass	39.082	−96.56	LAI-2000	BigFoot
3	Harvard forest	Broadleaf forest	42.538	−72.171	LAI-2000	BigFoot
4	Sevilleta	Shrubland	34.344	−106.671	LAI-2000	BigFoot
5	Tundra	Shrubland	71.268	−156.612	LAI-2000	BigFoot
6	Larose	Needleleaf forest	45.381	−75.217	Hemispherical photography	VALERI
7	Santa Rosa	Broadleaf forest	10.815	−85.615	LAI-2000	(Kalácska et al., 2005)
8	Priest River	Needleleaf forest	48.350	−116.833	Allometric & Ceptometer	(Duursma et al., 2003)
9	Prince Albert	Needleleaf forest	53.700	−106.200	LAI-2000	(Barr et al., 2004)
10	Talamanca	Broadleaf forest	9.594	−83.742	LAI-2000	(Hölscher et al., 2003)

ice, our climatology values are also between the LAI_QC < 128 and LAI_QC < 32. The profile of LAI_TSF is more approximate to the LAI_QC < 128 during winter and spring. The difference between LAI_QC < 32 and LAI_QC < 128 exposes the uncertainties existing in the original products.

The operational MODIS LAI algorithm uses six major biome types as *a priori* information to constrain the vegetation structural and optical parameter space: grasses and cereal crops, shrubs, broadleaf crops, savannas, broadleaf forests and needleleaf forests (Knyazikhin et al., 1998). As explained above, using the PFT is advantageous in representing landscapes. However, there exist some mismatches between the six biomes of the LAI products and the eleven PFTs. This may explain part of the differences in the deciduous broadleaf trees, urban and built-up, and snow and ice types (Fig. 6d, i and j).

3.3. Comparison with the SG filter

The seasonal MODIS LAI products after SG filtering for both 2000 and 2001 are shown in Figs. 4b and 5a, respectively. The SG filter is good at providing a temporally continuous LAI profile over the season. This trait also helps to fill some mixing pixels spatially.

The SG filter greatly improved the poor MODIS LAI data at higher latitudes (> 50°) caused by clouds. Improvements are also observed in the Florida panhandle and the Alaska peninsular. In general, the LAI_SG results (Fig. 4b) are closer to the original LAI values than the TSF method (Fig. 4c), for example, in the Great Lakes regions. For broadleaf crops, the LAI_SG is about 1.0–1.5 higher than the MODIS standard LAI. This overestimation is quite similar to the TSF results. However, there are still some missing pixels, especially at higher latitudes (Fig. 4b). This problem is inherent to the SG method because it is essentially a temporal filter. The TSF method resolved this issue by taking into account the spatial distribution of LAI for different PFT (Fig. 4c). On day 169, 2001, the MODIS LAI was missing. Both SG and TSF reconstructed the LAI successfully (Fig. 5). The SG results have a higher spatial dynamic compared to the TSF. The SG values are higher than those of the TSF in the eastern United States, but are similar in the western states. For evergreen needleleaf trees, the SG results are also a little higher. The SG filter can give different results by altering the coefficients, but it still cannot provide quality spatially continuous products since it only takes into account values in the temporal neighborhood. The spatial correlations are not considered by the SG filter.

The climatology of the LAI_SG was also compared with other results (Fig. 6). For the LAI_SG curve, we did not separate the main radiative transfer and the backup retrieval algorithms. The LAI_SG curve approximates more closely the overall MODIS LAI profile than the best LAI (QC < 32). In general, the LAI_SG is higher than the LAI_TSF in summer and fall, but lower than the latter in winter and spring, especially for the trees. For the evergreen broadleaf trees, the LAI_SG is higher than the LAI_TSF for the whole season. For snow and ice, the LAI_SG is consistently lower than the MODIS LAI. Although we did not do any *posterior* adjustment, the SG algorithm will easily lead to overestimation for many cover types. Comparatively, the TSF did a better job restoring the spatial and temporal distribution of seasonal LAI trend.

3.4. Mean LAI for different latitude zones

Fig. 7 shows time series of LAI in 2001, represented by average LAI values within 10° latitude bands. A very regular annual cycle of vegetation growth is observable in the figure. In general, LAI_QC < 32 is lower than the curve of LAI_QC < 128. This indicates the potential overestimation of the backup vegetation index method. After filtering, the new LAI product

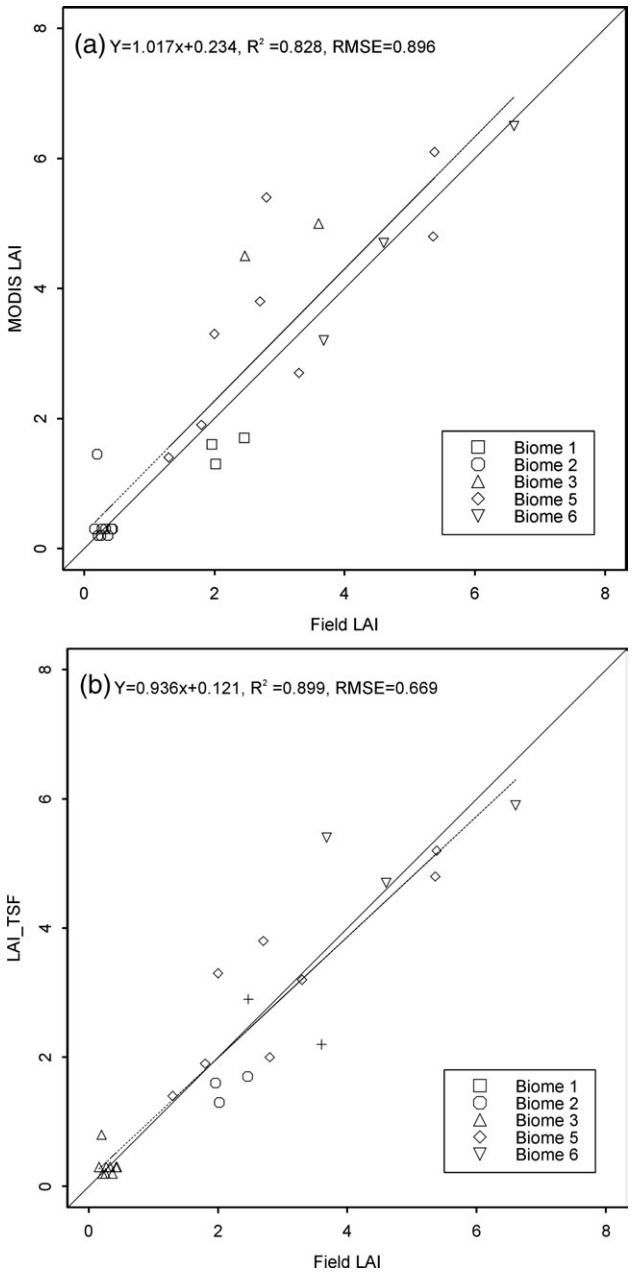

Fig. 8. Scatterplot of MODIS LAI (a) and filtered LAI (b) versus field measured LAI over ten sites listed in Table 3. The solid line is 1:1 line and the dashed line the regression line. The biome types are (1) grasses and cereal crops, (2) shrubs, (3) broadleaf crops, (5) broadleaf forests and (6) needleleaf forests, respectively.

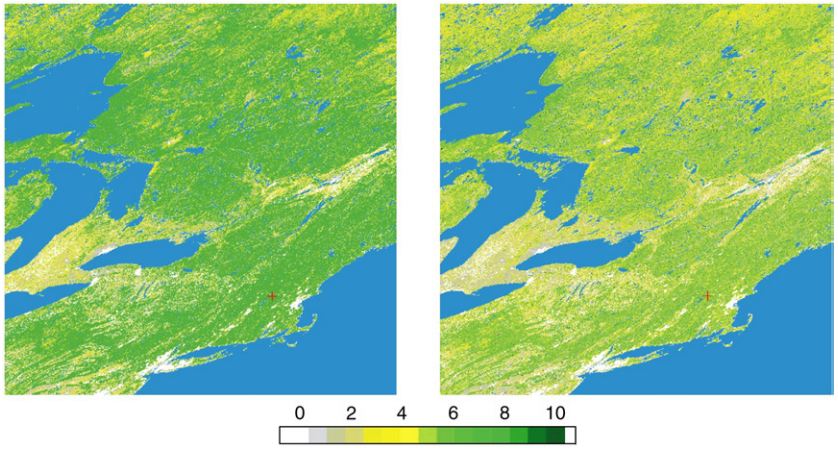

Fig. 9. The MODIS standard LAI product (a) and the results after TSF (b) for tile h12v04 on day 209, 2001 (1200 km × 1200 km). The red cross is where the HARV site is located.

filled the gaps and valleys in the MODIS products. Both SG and TSF provide temporally continuous curves for LAI. The LAI_SG curve is similar to the LAI_QC < 128 curve, while the LAI_TSF curve is similar to the LAI_QC < 32 curve.

In the 10°–20° latitude zone, the LAI is consistently around 3.0 over the year, higher than its value at all other latitudes in North America. This is reasonable because of the dominance of evergreen broadleaf trees in this latitudinal zone. At high latitudes (70°–80°), LAI is less than 0.5 for most of the year, coinciding with the sparsely vegetated areas of this region. For other latitudinal zones, the seasonal distribution of LAI is clear. They display a summer plateau and a winter valley, corresponding to the vegetation green-up and senescence in the Northern hemisphere.

4. Comparison with other data sets

The new LAI products are compared with other LAI data acquired at different levels. They are first validated with ground measured LAI data over North America. They are then compared with LAI estimated from Landsat ETM+ data. Finally, we compared the new LAI products with the monthly MODIS LAI composite data.

4.1. Comparison with in situ measurements

Ten field LAI measurements sites over North America have been selected for evaluation of the filter performances (Table 4). Five sites are from the BigFoot network (Cohen et al., 2000–2004a) and one site belongs to the VALERI project (Baret et al., 2006). Other four additional sites from the literature are also used. A total of 25 observations were obtained as some sites have multiple observations during the season. Different LAI measurement methods have been used in the field (Table 4). These points were each reprojected to the corresponding MODIS LAI and LAI_TSF products, respectively.

A good agreement between MODIS LAI and field measurements is observed (R^2 = 0.828 and RMSE = 0.896) for all biomes (Fig. 8a). The disagreement is slightly larger for a few broadleaf and needleaf forest points. The largest discrepancy reaches 2.6 at a broadleaf forest site (Santa Rosa). The filtered LAI (Fig. 8b) agree fairly better with the ground measurements (R^2 = 0.899 and

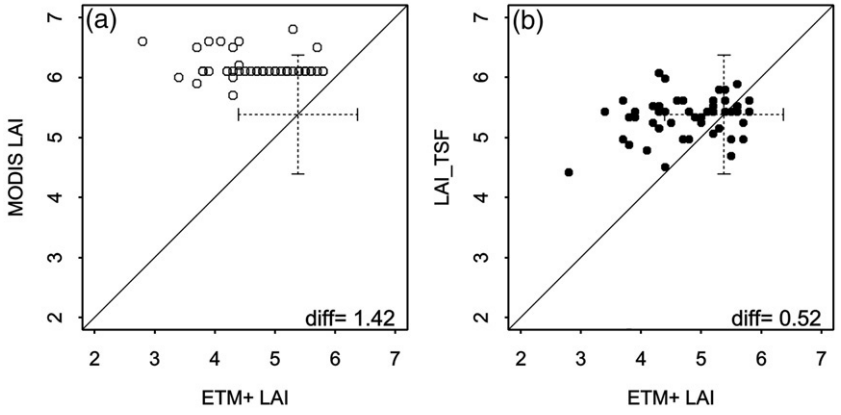

Fig. 10. Comparison of MODIS LAI and ETM+ LAI (a), and LAI_TSF and ETM+ LAI (b) at the HARV site (Jul 28, 2001). The dashed cross shows the measured mean value and the standard deviation. "diff" is the mean differences of MODIS LAI and LAI_TSF to ETM+ LAI, respectively. The hollow points in (a) indicate that all LAI are retrieved with the backup algorithm.

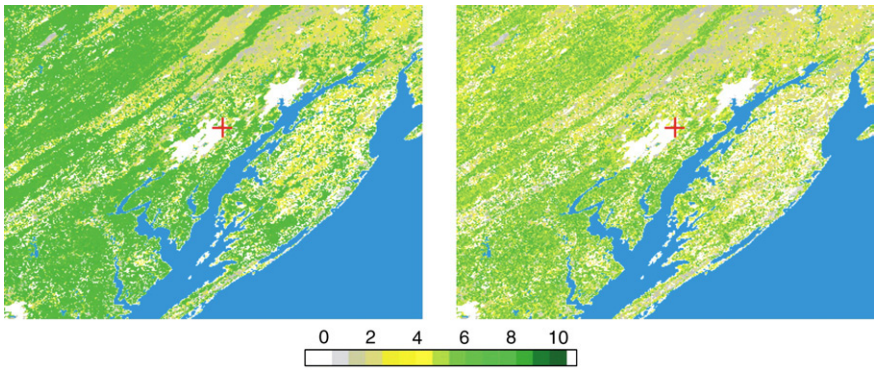

Fig. 11. The MODIS standard LAI product (a) and the results after TSF (b) for the BARC region on day 217, 2001 (400 × 300 km). The red cross shows the location of the BARC site.

RMSE = 0.669). One possible reason for the discrepancy is that the in situ field observation may not be representative of the overall MODIS pixel due to the heterogeneous ground conditions. More definitive conclusion on the accuracy of the reprocessed LAI could be drawn with more validation points.

4.2. Comparison with ETM+ and field LAI

We compared the new LAI products with the LAI data derived from Landsat ETM+ at two of the EOS land validation core sites (Morisette et al., 2002). The first one is the Harvard forest (HARV) site (42.538°, −72.171°) located in Massachusetts, USA. It is mainly covered by deciduous broadleaf forest. The other one is the Beltsville Agricultural Research Center (BARC) site (39.03°, −76.85°) located in Maryland, USA. The land cover types at BARC site are temperate broadleaf forests and agricultural lands. In both sites, ETM+ LAI data have been validated with field measurements (Cohen et al., 2003; Fang & Liang, 2003). The ETM+ LAI data were up-scaled to the MODIS resolution (1 km) with a spatial average sampling method and compared with the MODIS LAI and the TSF products, respectively.

4.2.1. Harvard forest site

Fig. 9 shows the MODIS standard LAI product (9a) and the results after TSF (9b) for tile h12v04 on July 28, 2001 (DOY 209). The retrieval index for this tile is only 0.32. In general, the TSF method produced lower LAI than the MODIS LAI. The distribution of the LAI_TSF is consistent with the landscape patterns. The LAI surfaces at Harvard forest were produced from the ETM+ image acquired on July 26, 2001 (DOY 207) (Cohen et al., 2000–2004b). The orthogonal RMA (Reduced Major Axis) regression method was used (Cohen et al., 2003). The ETM+ surface has a grain of 25 m and covers a 7 × 7 km extent. The MODIS LAI data (DOY 209, 2001) at this site were all retrieved with the backup algorithm due to cloud effect. Field measurements at this site were taken around the satellite overpass days (Gower, 2000–2004).

The MODIS LAI and LAI_TSF data were registered to the ETM+ LAI maps (7 × 7 km) and they were compared in Fig. 10. The mean value of field data and their standard deviation are shown with a cross. The field LAI is shown as a reference. The mean differences of MODIS LAI and LAI_TSF to ETM+ LAI are calculated. Both MODIS LAI and LAI_TSF overestimated the ETM+ LAI, but the TSF points fall closer to the 1:1 line, indicating that the TSF results have improved the MODIS standard LAI. MODIS LAI overestimated ETM+ LAI by 1.42 at this site (Fig. 10a). All MODIS LAI values are higher than the

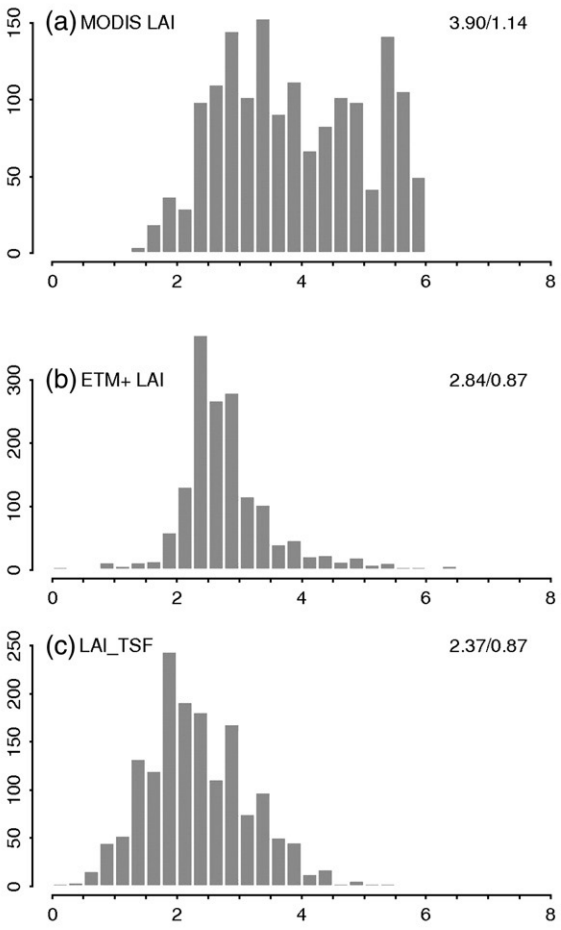

Fig. 12. Histogram comparison of broadleaf crop pixels by the MODIS backup algorithm in the BARC site (Aug 2, 2001). (a) the MODIS LAI products, (b) ETM+ LAI, and (c) the TSF processed LAI data The *x*-axis is the LAI values. The numbers at the upper right corner are the mean and standard deviation, respectively.

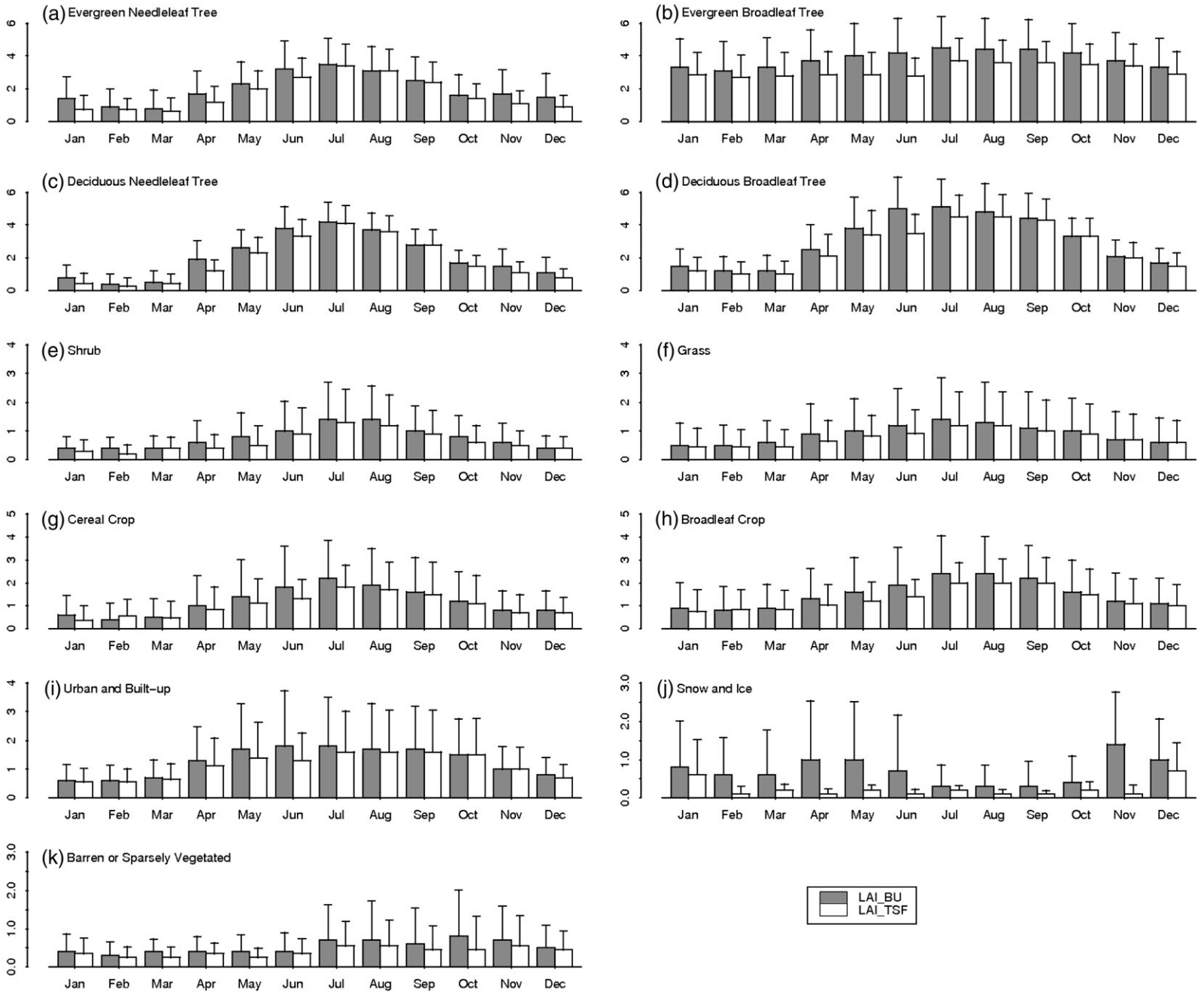

Fig. 13. Comparison of monthly mean LAI and the standard deviation for different plant functional types over North America. LAI_BU is the monthly LAI composite data from Boston University. LAI_TSF is from this paper. Year: 2001.

Table 5
Yearly mean LAI calculated from the BU and TSF monthly composites for different PFT

PFTs	1	2	3	4	5	6	7	8	9	10	11
LAI_BU	2.02	3.84	2.08	3.05	0.77	0.9	1.18	1.53	1.27	0.7	0.52
LAI_TSF	1.69	3.14	1.82	2.69	0.63	0.78	1.01	1.31	1.13	0.22	0.4
Difference	0.33	0.7*	0.26	0.36	0.14	0.12	0.17	0.22	0.14	0.48*	0.12*
R^2	0.949	0.58	0.976	0.938	0.942	0.918	0.943	0.946	0.923	0.052	0.754

The mean difference and R^2 of the two data sets are also shown. PFTs 1–11 correspond to (a)–(k) in Fig. 13.
* Significant at the 0.1 level.

mean field measured value. The average difference between LAI_TSF and ETM+ is 0.52 (Fig. 10b), less than the deviation of MODIS LAI. There is an outlier point ([3.8, 1.9], out of Fig. 10b) that has a very low value. This is the only point that has a valid MODIS LAI retrieved with the main radiative transfer method (in year 2002) over the 7×7 km region in five years. This value was used as the background x_b leading to the underestimation of LAI_TSF compared with ETM+ LAI in this point. For other points, the LAI_TSF and ETM+ LAI agree very well.

4.2.2. Beltsville Agricultural Research Center site

The MODIS standard LAI for the BARC region is shown in Fig. 11, together with the filtered results. The ETM+ LAI data of this site were derived from the aggregated ETM+ 510 m surface reflectance with a hybrid approach (Fang & Liang, 2005). These data have shown very good agreement with field measurements over the region. For broadleaf crops, the MODIS LAI products, derived from the main algorithm, agree well with both ETM+ LAI and field measurements (Fang & Liang, 2005). The errors are mainly observed in pixels with the backup retrieval algorithm. These errors can be corrected with the TSF method (Fig. 12). Fig. 12a shows the distribution of the original MODIS LAI for broadleaf crops retrieved with the backup algorithm. The MODIS LAI data have overestimated the ETM+ LAI (Fig. 12b) by about 1.0. On Aug 2, 2001, 25% of broadleaf crops were retrieved with the backup algorithm. There are more than 45.5% pixels located at the higher end (≥4.0) of the LAI span. Fig. 12c demonstrates that the TSF algorithm has greatly improved the LAI values for broadleaf crops. The histogram of the TSF results is very similar to the ETM+ LAI. Their mean values (2.37 vs. 2.84) are alike and the standard deviations (0.87 vs. 0.87) are the same.

The MODIS LAI overestimated broadleaf forests in this site by about 2.0–3.0 (Fang & Liang, 2005). However, the improvements of the TSF algorithm for broadleaf forests are not as significant as for other cover types. This can be attributed to the low quality of the MODIS products for broadleaf forests, even with the main RT algorithm. Currently, the MODIS science team is working toward improving the LAI estimation for broadleaf forests that will be distributed in collection 5 (Shabanov et al., 2005). We are expecting enhanced TSF performance over broadleaf forests when the new products are used.

4.3. Comparison with monthly composite data

To analyze the quality of the reprocessed data we compared our data with the latest monthly LAI composite data provided by Boston University (http://cliveg.bu.edu and ftp://primavera.bu.edu/pub/datasets/MODIS/) in Fig. 13. For each monthly composite, there are four 8-day LAI and QC values from MOD15A2 product (days 121 and 241 are used twice). If at least one of the inputs has QC<32, the composite value is the average of all high quality inputs. If none of the input has QC<32, the output LAI is assigned the value corresponding to the maximum FPAR. The TSF monthly composites are produced in a similar fashion. The monthly composites are representative of the LAI amplitude for North America in a given year. The mean LAI data from the two methods display typical patterns of LAI time series for different PFT (Fig. 13). For example, the crops show a clear seasonal green-up and senescence mode while there is considerable scatter amongst the snow and ice pixels over the year, especially during the spring and winter seasons. There is a high correlation between the two data sets for most PFTs (Table 5). Moreover, for three PFTs, the evergreen broadleaf tree, snow and ice, and the barren or sparsely vegetated, the monthly mean LAI of the BU composites are significantly higher values than those of the TSF data sets. Among all PFTs, the evergreen broadleaf tree shows the biggest difference where the BU composite is 0.7 higher than the TSF data. The large difference could be due to the field complexity of the evergreen broadleaf trees. The monthly LAI of the evergreen broadleaf trees bears a higher STD than other PFTs (Fig. 13). Moreover, the multi-year STD of the evergreen broadleaf tree is also very high (Fig. 1). The TSF algorithm takes into account the multi-year average and thus will mitigate the high deviation for a certain year (2001). The MODIS LAI is also known for its overestimation of wood vegetation because of algorithm deficits (Myneni et al., 2005; Shabanov et al., 2005). For the evergreen broadleaf trees, about 37.8% pixels are retrieved by the backup algorithm and 23.1% pixels have no valid retrieval (Table 3), which partly explains the overestimation of this plant functional type. For other PFTs, the LAI estimates of the BU composites are only slightly higher than the LAI estimates of the TSF data. The small difference is to be expected since both data sets are assembled from the best QC data.

5. Conclusion

There are large numbers of low quality and missing LAI values in the original MODIS products due to atmospheric or instrument effects. A temporal spatial filtering (TSF) method was designed to produce spatially and temporally complete products. The new LAI products are derived from the highest quality MODIS LAI products. Both low quality data and missing values are filled with the new estimates from the highest quality data.

Results in this paper have shown that the TSF method is able to reconstruct higher quality LAI time series products efficiently. Climatologies of the new spatially complete LAI products were calculated based on different plant functional types (PFT). The new LAI products illustrate clear seasonal trends for different PFTs and latitude zones. Statistics from the continuous LAI products should improve our understanding of the spatial distribution of LAI.

The TSF results were compared with the Savitzky–Golay (SG) filter. The TSF outperformed the SG filter in reconstructing the distribution of LAI, both spatially and temporally. The SG filter should be used cautiously to produce continuous LAI time series, especially during the vegetation–growing season. In contrast, our TSF algorithm is more robust and can be executed automatically.

The TSF algorithm not only provides continuous products but also improves the original data quality. This has been demonstrated through comparison with ETM+ LAI and field measurements at the HARV (broadleaf forest) and BARC (mixed broadleaf forest and crop) sites. Our monthly composited data and the MODIS LAI monthly composites agree very well for most PFTs since both are derived from the best QC data. For the two monthly data sets, significant differences exist for the evergreen broadleaf forest, snow and ice, and the barren or sparsely vegetated. It is acknowledged that more extensive validation work is necessary for an in depth understanding of the TSF method to produce continuous high-quality data products. Although this method was implemented only over North America, it will be straightforward to apply it globally with additional resources.

Acknowledgements

The work is supported by NASA Grant NNG04GL85G. The value-added LAI products will be available at the Global Land Cover Facility (GLCF) of the University of Maryland (http://glcf.umiacs.umd.edu/). We thank Dr. W. Cohen (Oregon State University) and the BigFoot science team (http://www.fsl.orst.edu/larse/bigfoot/index.html) who made field measurements and the LAI products from ETM+ available to the public. We also thank the support team at the Land Processes Distributed Active Archive Center (DAAC) (http://LPDAAC.usgs.gov), who helped set up the Machine-to-Machine Search and Order Gateway (MTMGW) which greatly facilitated the MODIS data downloading from the EROS Data Center (EDC).

References

Barr, A. G., Black, T. A., Hogg, E. H., Kljun, N., Morgenstern, K., & Nesic, Z. (2004). Inter-annual variability in the leaf area index of a boreal aspen–hazelnut forest in relation to net ecosystem production. *Agricultural and Forest Meteorology*, *126*(3–4), 237−255.

Baret, F., Weiss, M., Garrigue, S., Allard, D., Guinot, J.P., Leroy, M., Jeanjean, H., Bohbot, H., Bosseno, R., Dedieu, G., Bella, C.D., Espana, M., Gond, V., Gu, X.F., Guyon, D., Lelong, C., Mougin, E., Nilson, T., Veroustraete, F., Vintilla, R., submitted for publication. VALERI: A network of sites and a methodology for the validation of medium spatial resolution land satellite products. Remote Sensing of Environment.

Bergthorsson, P., & Doos, B. (1955). Numerical weather map analysis. *Tellus*, *7*, 329−340.

Berterretche, M., Hudak, A. T., Cohen, W. B., Maiersperger, T. K., Gower, S. T., & Dungan, J. (2005). Comparison of regression and geostatistical methods for mapping Leaf Area Index (LAI) with Landsat ETM+ data over a boreal forest. *Remote Sensing of Environment*, *96*(1), 49−61.

Bonan, G. B., Levis, S., Kergoat, L., & Oleson, K. W. (2002). Landscapes as patches of plant functional types: An integrating concept for climate and ecosystem models. *Global Biogeochemical Cycles*, *16*(2) 5-1−5-25.

Chen, J., Jönsson, P., Tamura, M., Gu, Z., Matsushita, B., & Eklundh, L. (2004). A simple method for reconstructing a high quality NDVI time-series data set based on the Savitzky–Golay filter. *Remote Sensing of Environment*, *91*(3–4), 332−344.

Cihlar, J. (1996). Identification of contaminated pixels in AVHRR composite images for studies of land biosphere. *Remote Sensing of Environment*, *56*(3), 149−163.

Cohen, W. B., Maiersperger, T. K., & Pflugmacher, D. (2000–2004). *LAI Surface for BigFoot MODIS Land Product Validation Dataset.* Oak Ridge, Tennessee, U.S.A.: Oak Ridge National Laboratory Distributed Active Archive Center.

Cohen, W. B., Maiersperger, T. K., & Pflugmacher, D. (2000–2004). *LAI Surface for BigFoot MODIS Land Product Validation, HARV 2001 Dataset.* Oak Ridge, Tennessee, U.S.A.: Oak Ridge National Laboratory Distributed Active Archive Center.

Cohen, W. B., Maiersperger, T. K., Yang, Z., Gower, S. T., Turner, D. P., Ritts, W. D., et al. (2003). Comparisons of land cover and LAI estimates derived from ETM+ and MODIS for four sites in North America: A quality assessment of 2000/2001 provisional MODIS products. *Remote Sensing of Environment*, *88*(3), 233−255.

DeFries, R., Hansen, M., Townshend, J. R. G., Janetos, A. C., & Loveland, T. R. (2000). A new global 1 km data set of percent tree cover derived from remote sensing. *Global Change Biology*, *6*, 247−254.

Dungan, J. (1998). Spatial prediction of vegetation quantities using ground and image data. *International Journal of Remote Sensing*, *19*(2), 267−285.

Duursma, R. A., Marshall, J. D., & Robinson, A. P. (2003). Leaf area index inferred from solar beam transmission in mixed conifer forests on complex terrain. *Agricultural and Forest Meteorology*, *118*(3–4), 221−236.

Fang, H., & Liang, S. (2003). Retrieve LAI from Landsat 7 ETM+ data with a neural network method: Simulation and validation study. *IEEE Transactions on Geoscience and Remote Sensing*, *41*(6), 2052−2062.

Fang, H., & Liang, S. (2005). A hybrid inversion method for mapping leaf area index from MODIS data: Experiments and application to broadleaf and needleleaf canopies. *Remote Sensing of Environment*, *94*(3), 405−424.

Fang, H., Liang, S., McClaran, M. P., Leeuwen, W. V., Drake, S., Marsh, S. E., et al. (2005). Biophysical characteristics and management effects on semiarid rangeland observed from Landsat ETM+ data. *IEEE Transactions on Geosciences and Remote Sensing*, *43*(1), 125−134.

Gower, S. T. (2000–2004). *LAI field measurements for BigFoot MODIS Land Product Validation, HARV 2001 Dataset.* Oak Ridge, Tennessee, U.S.A.: Oak Ridge National Laboratory Distributed Active Archive Center.

Hansen, M., DeFries, R., Townshend, J. R., Carroll, M., Dimiceli, C., & Sohlberg, R. (2003). *500 m MODIS Vegetation Continuous Fields.* College Park, Maryland: The Global Land Cover Facility.

Haxeltine, A., & Prentice, I. C. (1996). BIOME3: An equilibrium terrestrial biosphere model based on ecophysiological constraints, resource availability, and competition among plant functional types. *Global Biogeochemical Cycles*, *10*, 693−709.

Hölscher, D., Köhler, L., Leuschner, C., & Kappelle, M. (2003). Nutrient fluxes in stemflow and throughfall in three successional stages of an upper montane rain forest in Costa Rica. *Journal of Tropical Ecology*, *19*, 557−565.

Jönsson, P., & Eklundh, L. (2002). Seasonality extraction by function fitting to time–series of satellite sensor data. *IEEE Transactions on Geoscience and Remote Sensing*, *40*(8), 1824−1832.

Kalácska, M., Calvo-Alvarado, J. C., & Sánchez-Azofeifa, G. A. (2005). Calibration and assessment of seasonal changes in leaf area index of a tropical dry forest in different stages of succession. *Tree Physiology*, *25*, 733−744.

Karnieli, A., Gabai, A., Ichoku, C., Zaady, E., & Shachak, M. (2002). Temporal dynamics of soil and vegetation spectral responses in a semi-arid environment. *International Journal of Remote Sensing*, *23*(19), 4073−4087.

Knyazikhin, Y., Martonchik, J. V., Myneni, R. B., Dine, D. J., & Running, S. W. (1998). Synergistic algorithm for estimating vegetation canopy leaf area index and fraction of absorbed photosynthetically active radiation from MODIS and MISR data. *Journal of Geophysical Research*, *103*, 32,257−32,276.

Moody, E. G., King, M. D., Platnick, S., Schaaf, C. B., & Gao, F. (2005). Spatially complete global spectral surface albedos: Value-added datasets derived from Terra MODIS land products. *IEEE Transactions on Geoscience and Remote Sensing*, *43*(1), 144−158.

Morisette, J. T., Privette, J. L., & Justice, C. O. (2002). A framework for the validation of MODIS Land products. *Remote Sensing of Environment*, *83* (1–2), 77−96.

Myneni, R., Yang, W., T.B, Shabanov, N., & Knyazikhin, Y. (2005). Global products of vegetation leaf area and fraction absorbed PAR from MODIS sensors onboard NASA Terra and Aqua satellites. In S. Liang, J. Liu, X. Li, R. Liu, & M. Schaepman (Eds.), *Proceedings of the 9th International Symposium on Physical Measurements and Signatures in Remote Sensing, Beijing, China*, *Vol. 1*. (pp. 200−202) Beijing (Oct. 17−19, 2005).

Running, S. W., & Gower, S. T. (1991). FOREST-BGC, a general model of forest ecosystem processes for regional applications, II, dynamic carbon allocation and nitrogen budgets. *Tree Physiology*, *9*, 147−160.

Running, S. W., & Hunt, E. R. (1991). Generalization of a forest ecosystem process model for other biomes. In J. R. Ehleringer & C.B. Field (Eds.), *Scaling Physiological Processes: Leaf to Globe* (pp. 141−158). San Diego, California: Academic.

Savitzky, A., & Golay, M. J. E. (1964). Smoothing and differentiation of data by simplified least squares procedures. *Analytical Chemistry*, *36*(8), 1627−1639.

Sellers, P. J., Tucker, C. J., Collatz, G. J., Los, S. O., Justice, C. O., Dazlich, D. A., et al. (1994). A global 1° by 1° NDVI data set for climate studies. Part 2: The generation of global fields of terrestrial biophysical parameters from the NDVI. *International Journal of Remote Sensing*, *15*, 3519−3545.

Shabanov, N. V., Kotchenova, S., Huang, D., Yang, W., Tan, B., Knyazikhin, Y., et al. (2005). Analysis and optimization of the MODIS leaf area index algorithm retrievals over broadleaf forests. *IEEE Transactions on Geoscience and Remote Sensing*, *43*(8), 1855−1865.

Small, C. (2004). The Landsat ETM+ spectral mixing space. *Remote Sensing of Environment*, *93*(1–2), 1−17.

Viovy, N., Arion, O., & Belward, A. S. (1992). The best index slope extraction (BISE): A method for reducing noise in NDVI time-series. *International Journal of Remote Sensing*, *12*, 1585−1590.

Wang, Y., Tian, Y., Zhang, Y., El-Saleous, N., Knyazikhin, Y., Vermote, E., et al. (2001). Investigation of product accuracy as a function of input and model uncertainties: Case study with SeaWiFS and MODIS LAI/FPAR algorithm. *Remote Sensing of Environment*, *78*(3), 296−311.

Yang, W., Huang, D., Tan, B., Stroeve, J. C., Shabanov, N. V., Knyazikhin, Y., et al. (2006). Analysis of leaf area index and fraction of PAR absorbed by vegetation products from the Terra MODIS sensor: 2000–2005. *IEEE Transactions on Geoscience and Remote Sensing*, *44*(7), 1829−1841.

Zhang, X., Friedl, M. A., Schaaf, C. B., Strahler, A. H., Hodges, J., Gao, F., et al. (2003). Monitoring vegetation phenology using MODIS. *Remote Sensing of Environment*, *84*(3), 471−475.